Modeling Cell-Specific Dynamics and Regulation of the Common Gamma Chain Cytokines

Ali M. Farhat[a,c], Adam C. Weiner[a,c], Cori Posner[b], Zoe S. Kim[a], Scott M. Carlson[b], and Aaron S. Meyer[a,d]

[a]*Department of Bioengineering, Jonsson Comprehensive Cancer Center, Eli and Edythe Broad Center of Regenerative Medicine and Stem Cell Research; University of California, Los Angeles*

[b]*Visterra, Inc., Waltham, MA*

[c]*These authors contributed equally to this work*

[d]*a@asmlab.org*

Abstract

Many receptor families exhibit both pleiotropy and redundancy in their regulation, with multiple ligands, receptors, and responding cell populations. Any intervention, therefore, has multiple effects and is context specific, confounding intuition about how to carry out precise therapeutic manipulation. The common γ-chain cytokine receptor dimerizes with complexes of the cytokines interleukin (IL)-2, IL-4, IL-7, IL-9, IL-15, and IL-21 and their corresponding "private" receptors. These cytokines have existing uses and future potential as immune therapies due to their ability to regulate the abundance and function of specific immune cell populations. Here, we build a binding-reaction model for the ligand-receptor interactions of common γ-chain cytokines enabling quantitative predictions of response. We show that accounting for receptor-ligand trafficking is essential to accurately model cell response. Using this model, we visualize regulation across the family and immune cell types by tensor factorization. This model accurately predicts ligand response across a wide panel of cell types under diverse experimental designs. Further, we can predict the effect of ligands across cell types. In total, these results present a more accurate model of ligand response validated across a panel of immune cell types, and demonstrate an

approach for generating interpretable guidelines to manipulate the cell type-specific targeting of engineered ligands.

Summary points

- A dynamical model of the γ-chain cytokines accurately models responses to IL-2, IL-15, IL-4, and IL-7.
- Receptor trafficking is necessary for capturing ligand response.
- Tensor factorization maps responses across cell populations, receptors, cytokines, and dynamics.
- An activation model coupled with tensor factorization creates design specifications for engineering cell-specific responses.

Introduction

Cytokines are cell signaling proteins responsible for cellular communication within the immune system. The common γ-chain (γ_c) receptor cytokines, including interlukin (IL)-2, 4, 7, 9, 15, and 21, are integral for modulating both innate and adaptive immune responses. As such, they have existing uses and future potential as immune therapies.[1,2] Each ligand binds to its specific private receptors before interacting with the common γ_c receptor to induce signaling.[3] γ_c receptor signaling induces lymphoproliferation, offering a mechanism for selectively expanding or repressing immune cell types.[4,5] Consequently, loss-of-function or reduced activity mutations in the γ_c receptor can cause severe combined immunodeficiency (SCID) due to insufficient T and NK cell maturation.[6] Deletion or inactivating mutations in IL-2 or its private receptors leads to more selective effects, including diminished regulatory T cell (T_{reg}) proliferation and loss of self-tolerance.[7–9] Deficiency in the IL-2 receptor IL-2Rα also causes hyperproliferation in CD8+ T cells, but diminished antigen response.[10] These examples show how γ_c receptor cytokines coordinate a dynamic balance of immune cell abundance and function.

The γ_c cytokines' ability to regulate lymphocytes can impact both solid and hematological tumors.[11] IL-2 is an approved, effective therapy for metastatic melanoma, and the antitumor effects of IL-2 and -15 have been explored in combination with other treatments.[12,13] Nonetheless, understanding these cytokines' regulation is stymied by their complex binding and activation mechanism.[3] Any intervention imparts effects across multiple distinct cell populations, with each population having a unique response defined by its receptor expression.[14,15] These cytokines' potency is largely limited by the severe toxicities, such as deadly vascular leakage with IL-2.[16] Finally, IL-2 and IL-15 are rapidly cleared by receptor-mediated endocytosis, limiting their half-life *in vivo*.[17,18]

To address the limitations of natural ligands, engineered proteins have been produced with potentially beneficial properties.[2] The most common approach has been to develop mutant ligands by modulating the binding kinetics for specific receptors.[19,20] For example, mutant IL-2 forms with a higher binding affinity for IL-2Rβ, or reduced binding to IL-2Rα, induce greater cytotoxic T cell proliferation, antitumor responses, and proportionally less T_{reg} expansion.[12,21] This behavior can be understood through IL-2's typical mode of action, in which T_{reg}s are sensitized to IL-2 by expression of IL-2Rα.[14] Bypassing this sensitization mechanism thus shifts cell-specificity.[21] Conversely, mutants skewed toward IL-2Rα over IL-2Rβ binding selectively expand T_{reg} populations, over cytotoxic T cells and NK cells, compared to native IL-2.[22,23]

The therapeutic potential and complexity of this family make computational models especially valuable for rational engineering. Early attempts at mathematically modeling the synergy between IL-2 and IL-4 in B and T cells successfully identified a phenomenological model that could capture the synergy between the two cytokines.[24] A cell population model has explained how T_{reg} IL-2 consumption suppresses effector T cell activation.[25] However, any model needs to incorporate the key regulatory features of a pathway to accurately predict cell response. With structural information that clarified the mechanism of cytokine binding, a model of IL-4, IL-7, and IL-21 binding revealed pathway cross-talk due to the relative γ_c receptor affinities.[26] Nevertheless, these models have failed to account for endosomal trafficking, and have not been constructed to model multiple immune cell types. IL-2 induces rapid endocytosis-mediated

IL-2Rα and IL-2Rβ downregulation,[14,27] and trafficking is known to be a potent regulatory mechanism for all members of the γ_c family.[28] Indeed, an early model showed the critical importance of IL-2 trafficking, but without the structural features of ligand binding enabling specific ligand engineering.[29]

In this paper, we assemble a map of γ_c cytokine family regulation. We first built a family-wide mathematical model that incorporates both binding and trafficking kinetics. This more comprehensive model allows us to investigate emergent behavior, such as competition between cytokines. This cytokine family is inherently high dimensional—with multiple ligands, cognate receptors, and cells with distinct expression. Therefore, we use tensor factorization methods to visualize the family-wide regulation. This map helps visualize how native or engineered ligands are addressed to specific immune cell populations based on their receptor expression levels. The methods used here can similarly be used in experimental and computational efforts of decoding other complex signaling pathways such as Wnt, Hedgehog, Notch, and BMP/TGFβ.[30–33]

Results

Trafficking is necessary to capture IL-2 and IL-15 dose response and the effect of IL-2Rα expression

To model how individual binding events give rise to cell response, we built a differential equation model representing the relevant binding and regulatory mechanisms within the γ_c receptor cytokine family (Fig. 1A). Binding interactions were modeled based on their known structural components, and led to the formation of receptor complexes capable of JAK/STAT signaling.[1] Endocytic trafficking of cell surface receptors is a critical mechanism of regulatory feedback.[29,34,35] Therefore, we extended earlier modeling efforts by including the trafficking of receptors and their complexes.[14,25] We assumed that species trafficked into an endosomal compartment while continuing to produce JAK/STAT signaling and participate in binding events.

Rate parameters for IL-2 and IL-15 binding events were parameterized by previous ex-

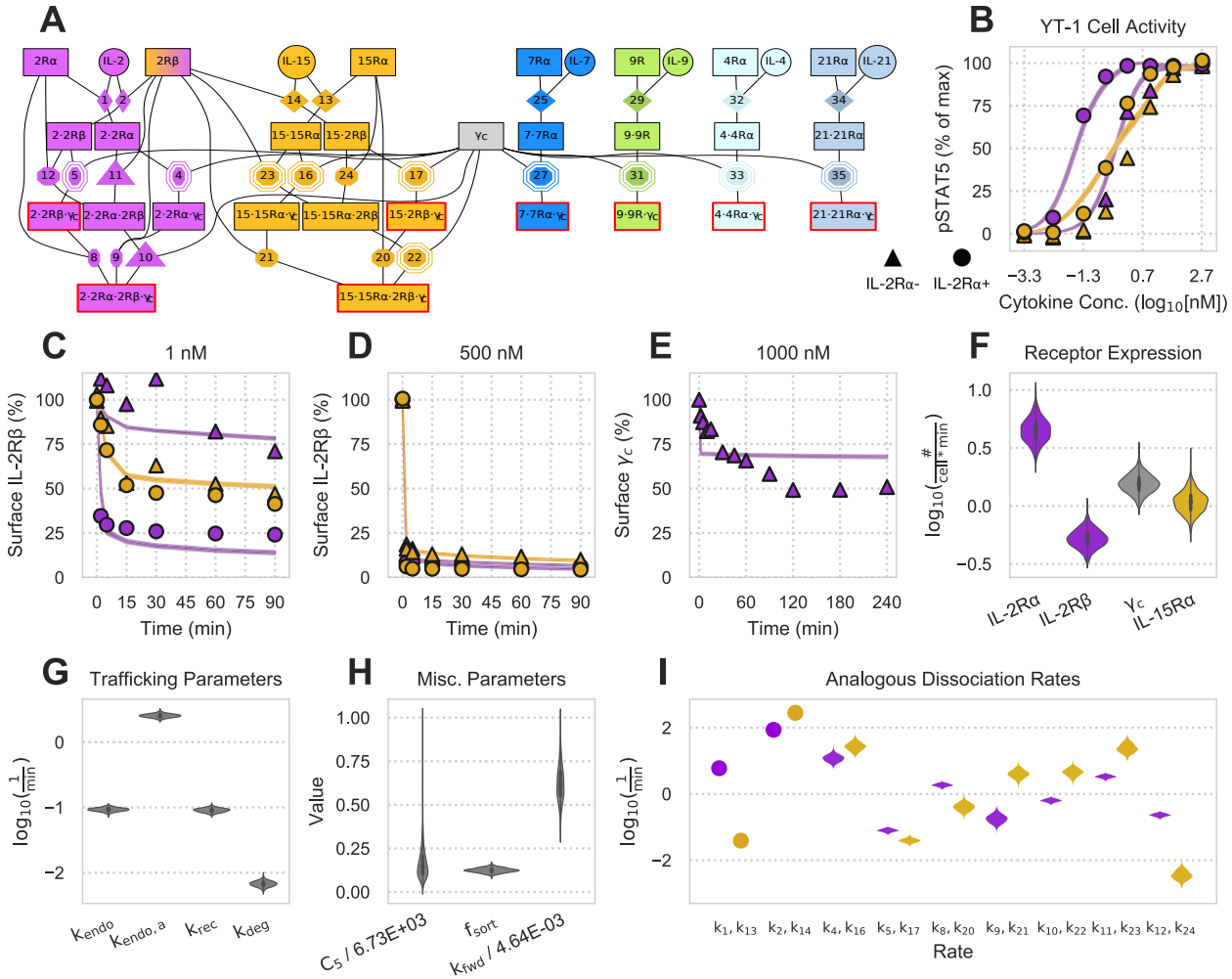

Figure 1: **Incorporating trafficking leads to an accurate model of IL-2 & IL-15 response.** A) Schematic of all receptor (boxes)-ligand (circles) complexes and binding events. Active (pSTAT5 signaling; containing two non-α receptors) complexes are outlined in red. Rate constants obtained from literature, detailed balance, or fitting are denoted by diamonds, octagons, or octagons with a double outline, respectively. Rate constants that were experimentally measured relative to other rates are denoted by triangles. B) Model prediction vs. experimental results for maximal pSTAT5 activation in YT-1 cells under various concentrations of ligand stimulation for 500 min. C-E) Model prediction vs. experimental results for percent of initial IL-2Rβ (C, D) and γ_c (E) on the cell surface for various ligand stimulation concentrations and cell types. The 25-75% and 10-90% confidence intervals of model predictions are shaded dark and light, respectively. F-H) Posterior distributions after data fitting. C_5 has units of $\# \times \text{cell}^{-1}$, k_{fwd} has units of $\text{cell} \times \#^{-1} \times \text{min}^{-1}$, and f_{sort} is unitless. I) Posterior distributions for the analogous reaction rates of IL-2 and IL-15. Rates constants measured in literature are represented by dots.

perimental measurements, detailed balance, or estimated by model fitting to existing experimental measurements (Fig. 1B–E). Fitting was performed to measurements of STAT5 phosphorylation and surface IL-2Rβ/γ_c, upon either IL-2 or IL-15 stimulation, in either wild-type YT-1 human NK cells or YT-1 cells selected for expression of IL-2Rα. The posterior parameter distributions from these fits (Fig. 1F–I) were plugged back into our model and showed quantitative agreement with the data, including differential sensitivity with IL-2Rα expression (Fig. 1B–F).[14,36] To evaluate the effect of including trafficking, we fit a version of the model without trafficking to the pSTAT5 measurements, using the same cell population as before; the model failed to capture differences with IL-2Rα expression even when using this limited fitting data (Fig. S1). Within the posterior distribution of parameter fits, IL-2·IL-2Rα complexes had a higher affinity for IL-2Rβ and γ_c than their IL-15·IL-15Rα counterparts in the trafficking model ($k_4 < k_{16}$ & $k_{11} < k_{23}$), consistent with prior work (Fig. 1I).[37] However, the opposite was true for IL-2Rβ ($k_4 > k_{16}$) and the affinities were equal for γ_c ($k_{11} = k_{23}$) in the no-trafficking model (Fig. S1B). Depletion of surface IL-2Rβ and γ_c occurs through rapid endocytosis of active complexes and indeed, depletion occurred faster at higher cytokine doses (Fig. 1C-E). Correspondingly, active complex internalization ($k_{endo,a}$) was inferred to be ~10x greater than that for inactive species (k_{endo}) (Fig. 1G). These data indicated that accounting for trafficking is essential for modeling IL-2 and IL-15 signaling response.

Since IL-2 and IL-15 drive the formation of analogous active complexes, with IL-2Rβ, γ_c, and a signaling-deficient high-affinity receptor (IL-2Rα/IL-15Rα), comparing their inferred binding rates gave insight into how IL-2 and IL-15 differ from one another (Fig. 1I). The two ligands had nearly the same direct binding affinity to IL-2Rβ; however, IL-15 had a higher affinity than IL-2 for its α-chain. Consequently, IL-15's complexes were inferred to more readily dimerize with a free α-chain than IL-2's complexes ($k_8 > k_{20}$, $k_{12} > k_{24}$). Similarly, IL-15 complexes had a slightly higher affinity for capturing IL-2Rβ/γ_c than their IL-2 counterparts ($k_9 < k_{21}$, $k_{10} < k_{22}$, $k_{11} < k_{23}$). The affinities of γ_c binding to ligand·IL-2Rβ and ligand·α-chain complexes were comparable between IL-2 and IL-15 ($k_4 = k_{16}$, $k_5 = k_{17}$). The data is also consistent with the literature in that both ligands have a higher affinity for IL-2Rβ when they are bound to their α-chain (k_2, $k_{14} > k_{11}$, k_{23}).[37] In total, a model of IL-2 and IL-15 incorporating trafficking is consistent with known biophysical and cell response measurements.

Family model correctly captures IL-4/IL-7 dose responses and cross-inhibition

To further test our model incorporating trafficking, we evaluated its performance in a series of experiments involving IL-4 and IL-7. IL-2 and IL-15 involve the same signaling-competent receptors and so the signaling activity of each cytokine cannot be distinguished. IL-4 and IL-7 activity, in contrast, can be distinguished when both cytokines are co-administered to cells since by measuring STAT6 and STAT5 phosphorylation, respectively.[2] Using this phenomenon we explored cross-inhibition data wherein IL-4 and IL-7 doses were administered to human PBMC-derived T cells ($CD4^+TCR^+CCR7^{high}$) both individually and together.[26]

Using surface abundance measurements of IL-4Rα, IL-7Rα, and γ_c, we applied a steady-state assumption in the absence of ligand to solve for each receptor expression rate.[26] Our model fits both single and dual cytokine dose-response data sets with high accuracy (Fig. 2B–C). The fitting process identifiably constrained reaction rates, trafficking parameters, and pSTAT scaling constants (Fig. 2F–I). Despite our surface abundance constraint, the receptor expression rates still formed distributions dependent on trafficking parameters (Fig. 2G–I).

The experimental data and model fits showed that IL-7 inhibited IL-4 activity more than IL-4 inhibited IL-7 activity (Fig. 2C).[26] Such inhibitory behavior was explained by the competition of ligand·α-chain complexes for the common γ_c. The K_d of this dimerization process for IL-7 (k_{27}) was smaller than the K_d for IL-4 (k_{33}), indicating that there was tighter dimerization of IL-7·IL-7Rα to γ_c than there was dimerization of IL-4·IL-4Rα to γ_c (Fig. 2F). The competition for γ_c was determined to play a larger role in signaling inhibition than receptor internalization since our model predicted that the same inhibitory relationships hold when active complexes internalize at the same rate as other species (Fig. 2D). Internalization was additionally dismissed because the majority of γ_c remained on the cell surface after ligand stimulation in both model simulation and experimental measurement (Fig. 2E).[26]

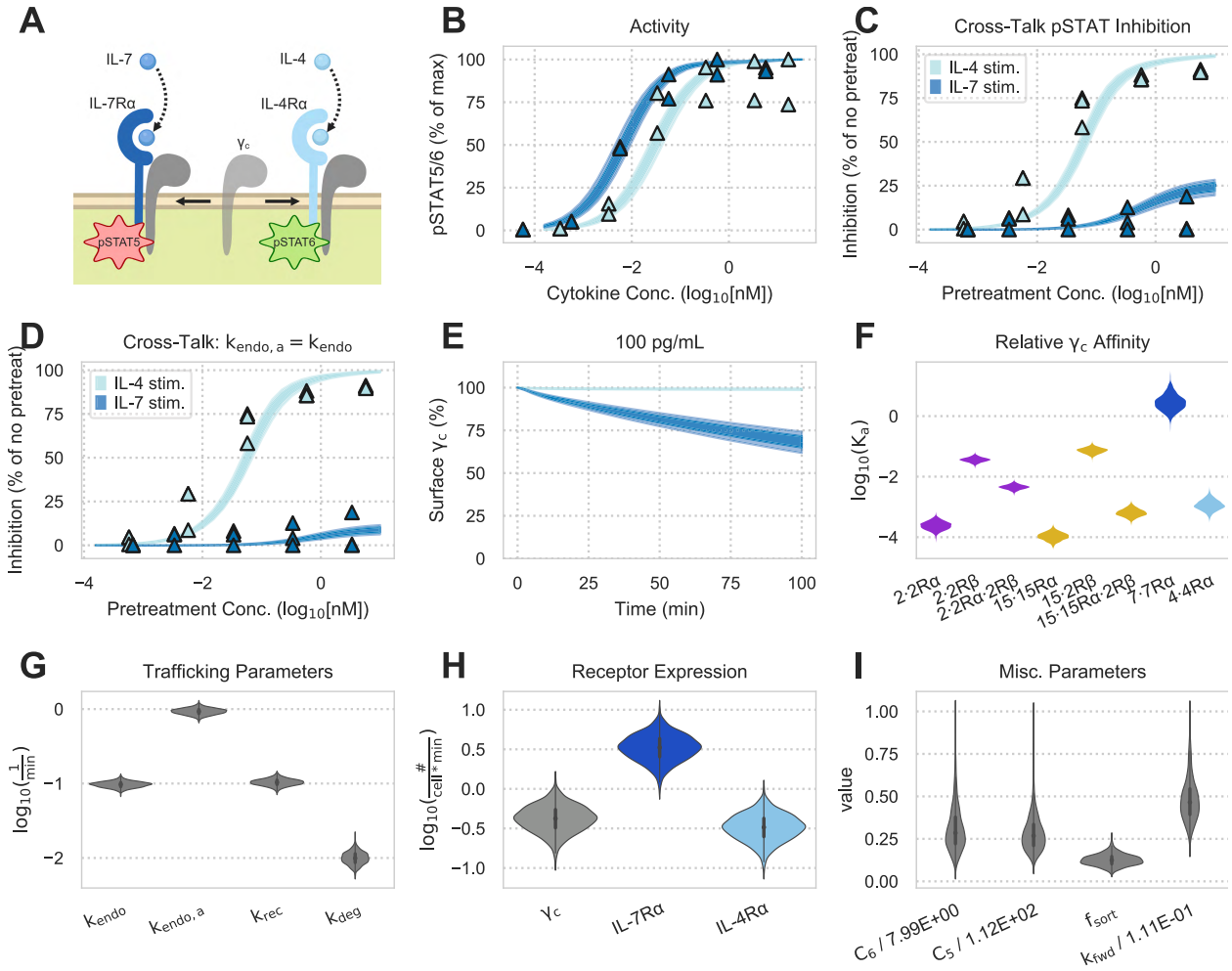

Figure 2: **A reaction model captures cytokine-cytokine interactions.** A) Schematic of IL-4 and IL-7 receptor complexes competing for γ_c and generating distinct pSTAT signals. B-C) Fitting model to experimental data. Experimental measurements are denoted by triangles. Shaded areas represent the 25-75% and 10-90% confidence intervals of model predictions. pSTAT5 and pSTAT6 were measured for IL-7 and IL-4 experiments, respectively. B) Single-cytokine pSTAT dose-response measurements for 10 min of exposure to IL-4 and IL-7. C) Percent inhibition of the second cytokine's pSTAT response in a dual-cytokine dose-response experiment. Human PBMC-derived T cells ($CD4^+TCR^+CCR7^{high}$) were pretreated with various concentrations of one cytokine for 10 min before being stimulated with a fixed concentration (50 pg/mL IL-7 or 100 pg/mL IL-4) of the other cytokine for an additional 10 min. D) Model predictions for percent inhibition of the second cytokine's pSTAT response in a dual-cytokine dose-response experiment with the assumption that active species are endocytosed at the same rate as inactive species ($k_{endo,a} = k_{endo}$). E) Model predictions for percent of γ_c on the cell surface when exposed to 100 pg/mL of either IL-7 or IL-4 for 100 min. F) Violin plot of K_a values obtained via posterior distributions of k_{fwd} / k_{rev} for k_{rev} parameters corresponding to different complexes competing for the common γ_c (Fig. 1A). G–I) Posterior distributions from fitting to data. C_5 and C_6 have units of $\# \times \text{cell}^{-1}$, k_{fwd} has units of $\text{cell} \times \#^{-1} \times \text{min}^{-1}$, and f_{sort} is unitless

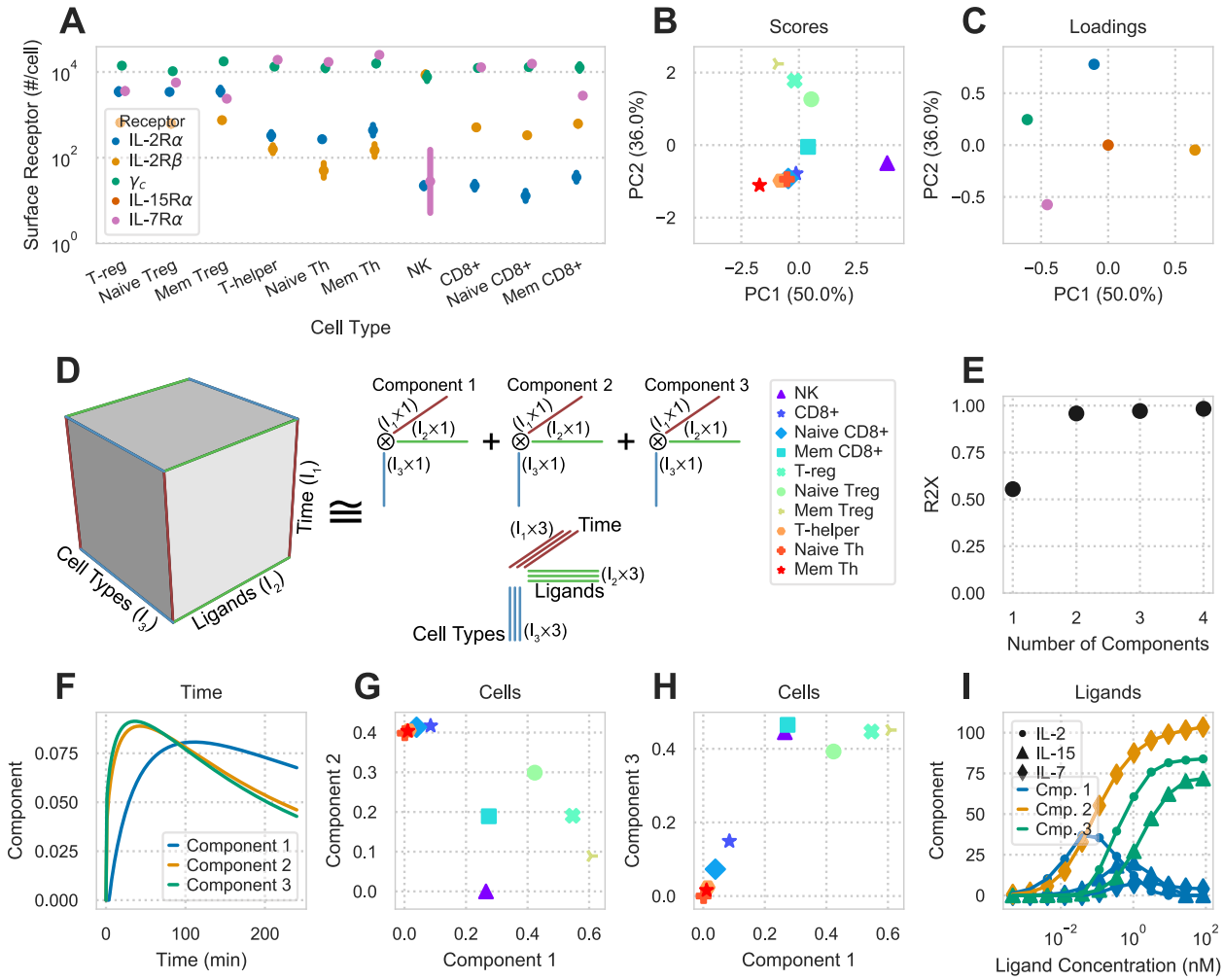

Figure 3: **Tensor factorization to map model-predicted cytokine responses.** A) Measured receptor abundance for ten PBMC-derived subpopulations. Points and error bars show geometric mean and standard deviation respectively (N = 4). Error bars for some points are too small to display. B-C) PCA scores (B) and loadings (C) of receptor abundance. Axis label percentages indicate percent variance explained. D) Schematic representation of CP decomposition. Model predictions are arranged in a cube depending upon the time, ligand treatment, and cell type being modeled. CP decomposition then helps to visualize this space. E) Percent variance reconstructed (R2X) versus the number of components used in non-negative CP decomposition. F-I) Component values versus time (F), cell type (G-H), or ligand stimulation (I). The variation explained by each component is the product of the component's time, ligand, and cell type factorization. Ligand components with only negligible values (< 5% max) are not shown.

Tensor Factorization Maps the Gamma Chain Family Response Space

Even with an accurate model, exploring dynamic responses across the many responding cell types and ligand treatments remains challenging. Restricting ones' view to a single time point, cell type, or ligand concentration provides only a slice of the picture. Therefore, we sought to apply factorization as a means to globally visualize ligand response.

As response to ligand is largely defined by receptor expression, we quantitatively profiled the abundance of each IL-2, IL-15, and IL-7 receptor across ten PBMC subpopulations (Fig. 3A). These data recapitulated known variation in these receptors, including high IL-7Rα or IL-2Rα expression in helper and regulatory T cells, respectively.[1,38] As mentioned above, IL-7 is uniquely able to cross-inhibit other γ_c cytokines, and excess IL-7Rα likely helps to ensure this occurs (Fig. 2).[26] Principal component analysis (PCA) helped visualize variation in these data (Fig. 3B-C). Principal component 1 most prominently separated the NK cells from all others due to their distinct receptor expression, with high levels of IL-2Rβ and relatively lower levels of γ_c. Principal component 2 then separated effector and regulatory T cell populations, based on their high IL-7Rα or IL-2Rα abundance, respectively. However, PCA also helped to identify slightly higher γ_c levels in T_{reg}s, and the slightly more T_{reg}-like profile of memory CD8+ cells.

To build a tensor of model predictions, we assembled simulation predictions across cell types, ligand conditions, and time. This three-dimensional (time, cell type, ligand) tensor was then decomposed with non-negative canonical polyadic (CP) decomposition (Fig. 3D). We selected three components during decomposition as this number captured 95% of the variance in our original data tensor (Fig. 3E). To show the relationships among the tensor's three dimensions, the component plots of each dimension were plotted alongside each other.

CP decomposition can be interpreted by matching a single component's effects across factor plots for each dimension. For example, component 2 is greatest at roughly 50 mins, for helper and CD8+ T cells, and almost exclusively with IL-7 stimulation (Fig. 3F–I). This indicates that this variation in the data occurs with IL-7 stimulation, leads to a response in helper and CD8+ T cells, and peaks at 50 minutes. In this way, different

contributory factors in cell response are separated.

Components 2 and 3 showed similar variation with time, peaking quickly and then decreasing after roughly 50 mins (Fig. 3F). This can be understood through two phases, in which receptor activation occurs, and then trafficking-mediated downregulation of the receptors (Fig. 1). Comparing the cells and ligands decomposition plots showed expected effects. IL-7 response was separated as component 2, showed a dose-dependent increase, and correlated with IL-7Rα expression levels (Fig. 3H–I). Interestingly, IL-2/IL-15 response separated by concentration, rather than ligand. Low concentrations of IL-2 were represented by component 1, and equally activated both regulatory and effector T cells (Fig. 3H–I). High concentrations of IL-2/IL-15 were represented by component 3 and activated effector T cells over regulatory ones (Fig. 3G, I). This known dichotomy occurs through higher IL-2Rα expression in T_{reg}s (Fig. 3A). The factorization also shows that the model predicts low-dose IL-2 stimulation to drive more sustained signaling than that from a high dose (Fig. 3F/I). Importantly, while PCA can help to distinguish cells based on distinct receptor expression profiles, cells separated differently based on their predicted ligand stimulation response (Fig. 3B/G/H). This demonstrates the benefit of tensor- and model-based factorization. Factorization highlighted a final possibility that T_{reg}s might be further discriminated by their combined IL-7 and IL-2 response (Fig. 3H). Efforts to selectively expand these cells could test this observation with combination ligand treatments.

Other tensor decomposition methods exist and can also be applied to visualize model-predicted response. For example, non-negative Tucker decomposition relaxes CP methods by employing a core tensor enabling interaction terms between components (Fig. S4).[39] However, this flexibility comes at the cost of interpretability, as visualizing the core tensor's effect is challenging. In total, factorization methods provide an effective means of visualizing the high-dimensional regulation of complex receptor families, including the influence of time, ligand stimulation, and receptor expression.

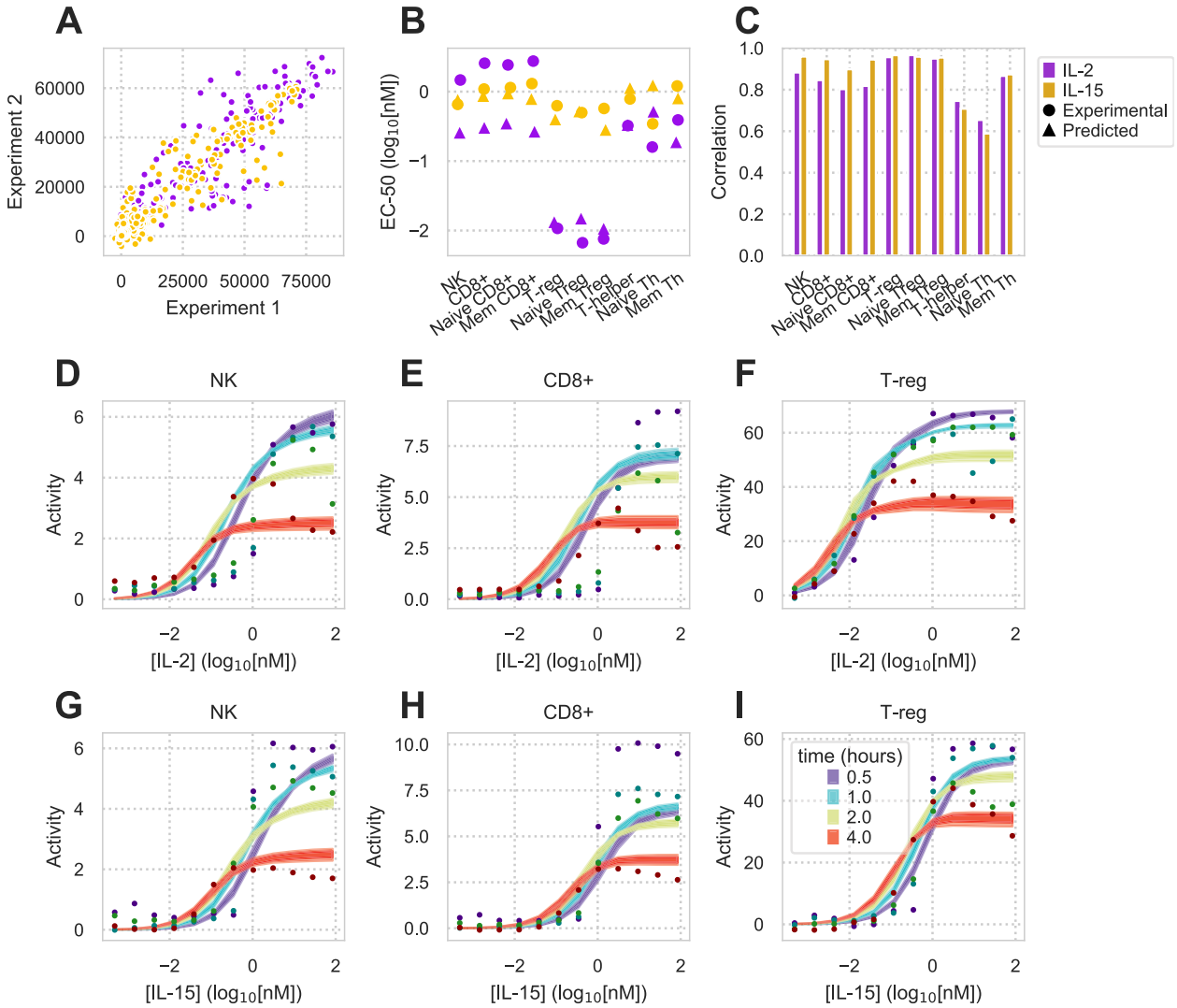

Figure 4: **Model accurately predicts cell type-specific response across a panel of PBMC-derived cell types.** A) Comparison of two replicates measuring pSTAT5 response to a dose-response of IL-2/15, time course, and panel of PBMC-derived cell types. B) Both experimentally-derived and model-predicted EC_{50}s of dose response across IL-2/15 and all 10 cell types. EC_{50}s are shown for 1 hr time point. C) Pearson correlation coefficients between model prediction and experimental measurements for all 10 cell populations (full data shown in fig. S5). D–I) pSTAT5 response to IL-2 (D-F) or IL-15 (G-I) dose responses in NK, CD8+, and T_{reg} cells.

Accurately Predicted Response Across a Panel of PBMC-Derived Cell Types

We evaluated whether our model could predict differences in the cell type-specificity of ligand treatment by comparing its predictions for IL-2/15 responses across our panel of 10 PBMC-derived cell populations. Overall, our model predictions of ligand pSTAT5 response closely matched experimental measurement (Figs. 4, S5). Individual cell types displayed reproducible responses to IL-2/15 treatment (Fig. 4A). The differences between cell types largely matched known differences in cytokine response. For example, T_{reg}s were markedly sensitive to IL-2 (Fig. 4B/F), but not IL-15 (Fig. 4B/I), at low concentrations of the cytokine.[22,23] Small amounts of of IL-2Rα in helper T cells (Fig. 3A) partially sensitizes them to IL-2 (Fig. 4B; Fig. S5H). The binding model accurately captured these differences in sensitivity and response across all the cell populations (Fig. 4C).

While the model accurately predicted experimentally-measured responses overall, and specifically the sensitivities of the dose-response profiles, we noticed some discrepancy specifically at high ligand concentrations, longer times, and specific cell populations (Fig. 4; fig. S5). For example, while CD8+ cells almost exactly match model predictions at 1 hr, by 4 hrs we experimentally observed a biphasic response with respect to IL-2 concentration, and a plateau with IL-15 that decreased over time. This decreased signaling was most pronounced with the CD8+ cells, but could be observed to lesser extents in some other cell populations such as NK cells (fig. S5). We hypothesize two possible explanations for this discrepancy: First, CD8+ populations are known to proteolytically shed IL-2Rα in an activity-responsive manner.[40] Our model also only uses a very simple sigmoidal relationship between active receptor and pSTAT5 signal. Other components of the Jak-STAT pathway surely influence its dynamic response.[41] However, overall the model presented here remains useful for exploring the determinants of cell type-specific response, which originate at the receptor expression profile on the cell surface.

Tensor Factorization of Experimental Measurements Distinguishes Cell Type-Specific Responses

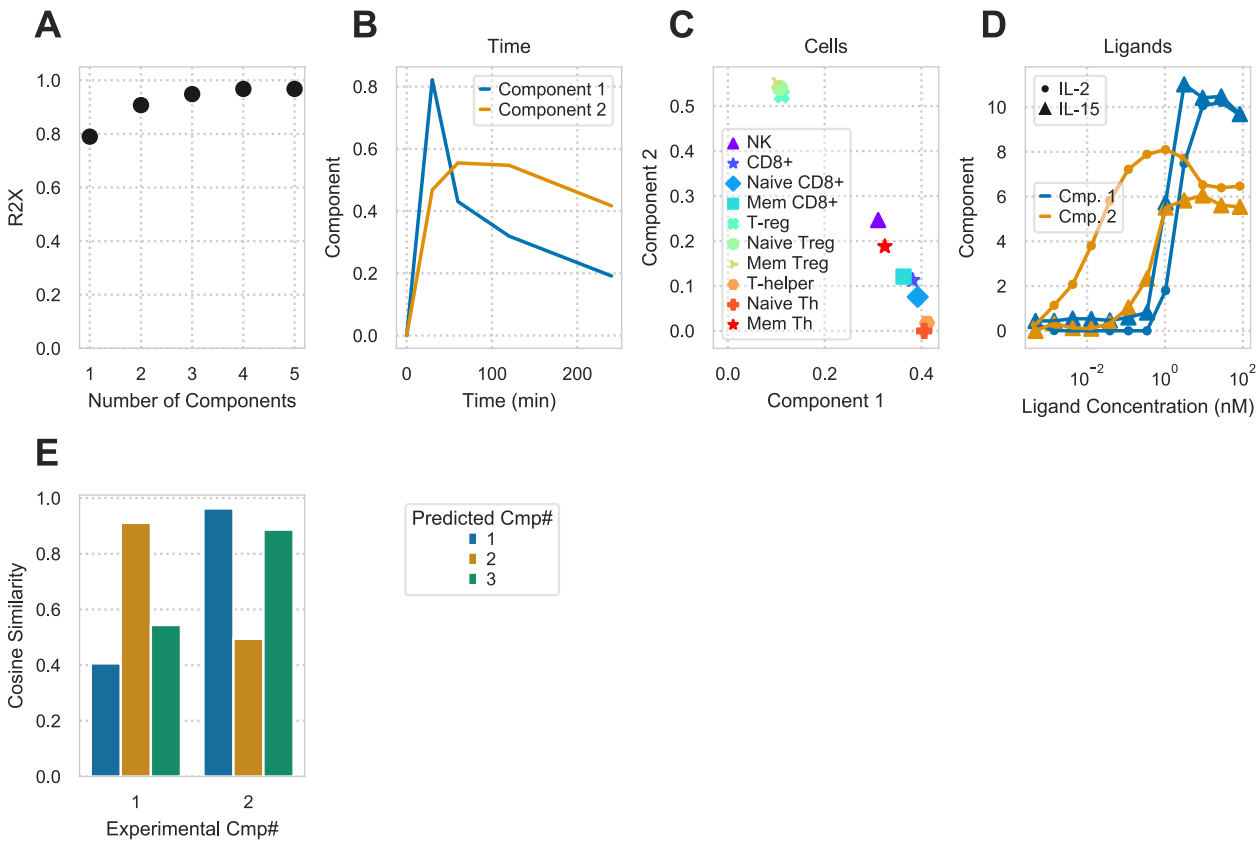

Figure 5: **Non-negative CP decomposition applied to experimental pSTAT5 measurements.** A) R2X of non-negative CP decomposition versus number of components used. B–D) Decomposition plot with respect to time (B), cell type (C), or ligand treatment (D). E) Pearson correlation coefficients between model and experimental cell type decomposition components.

Given that tensor factorization helped to visualize model predictions of IL-2, -7, and -15 response, we wished to evaluate whether it could similarly help to visualize experimental measurements. We structured our experimental pSTAT5 measurements in an identical format to the model simulation tensor Fig. 3. Factoring into two components explained roughly 90% of the variance in the original data (Fig. 5A), which we can then interpret using each of the factor plots (Fig. 5B–D).

Interestingly, these factors are distinguished by their concentration-dependence more so than being tied to a specific ligand (Fig. 5D). Component 2 only increases with low concentrations of IL-2, while component 1 increases at high concentrations of either ligand. As expected, effector and regulatory T cells are most strongly associated with

components 1 and 2, respectively, matching their known dose-response profiles (CITE) (Fig. 4). However, component 2 is also distinct from 1 in its sustained activation (Fig. 5B; Fig. S5), as predicted (Fig. 3F). This can be expected from rapid endocytosis-mediated downregulation of IL-2Rβ at high IL-2/15 concentrations (Fig. 1). Thus, tensor factorization helps to separate these differences in dose- and cell type-specific responses, as well as how they interact. Furthermore, cell type decomposition components showed positive correlations between specific experimental and predicted pairs while not in others; these components were responsible for T cell effector- and regulatory-specific signaling (Fig. 3G-I) (fig. 5E).

Discussion

Here, we built a mass-action kinetic binding model for the common γ_c receptor family, and used factorization methods to explore its cell type-dependent behavior. This approach provided insights into its high-dimensional regulation. Our binding-reaction model combined the structure of ligand interaction with endosomal trafficking, both of which are critical for accurately modeling response. This model was then able to predict IL-2 and -15 response across a wide panel of PBMC-derived cell types. Mass-action models can help to explain counter-intuitive features of ligand response and identify specific strategies for optimizing therapeutically-desired properties.[42,43] In the case of the γ_c receptor cytokines, a therapeutic goal has been to specifically modulate subpopulations of cells based on their unique receptor expression profiles.[12,21–23] To visualize these possibilities, we employed tensor factorization to map the signaling response space. This map provided a clearer picture of differential responsiveness between ligands, with selective and increased activation for certain cells and ligands over others. For example, we could clearly identify the selectivity of T helper cells for IL-7, and low concentrations of IL-2 for T_{reg}s.

The model described here serves as an effective tool for cell type-selective rational cytokine design. In addition to the natural ligands, many cytokine muteins have been designed with altered binding affinities to specific receptors.[19,20] Our model serves as a computational tool for screening these muteins as immunotherapeutic drugs that

selectively activate certain cell populations over others. For example, IL-2 muteins have shown therapeutic improvement over their wild type counterparts by drastically altering their binding affinities to either preferentially bind to IL-2Rα or IL-2Rβ/γ_c; these muteins were successful in selectively directing regulatory or effector T cell proliferation.[44] Models incorporating the full panel of responding cell populations will enable further refinement of these engineered ligands.[45] Both IL-2 and IL-15 have extremely short half-lives *in vivo*, in part due to endocytosis mediated clearance.[17,18] Including endocytic trafficking of ligand should enable future work modeling ligand clearance *in vitro* and *in vivo*. Changes in receptor binding may therefore be selected based on both optimized selectivity and pharmacokinetic properties. While cell types were defined here by their average receptor expression, cell-to-cell variability within these populations leads to variation in stimuli response.[15] Incorporating single cell variation will provide a more complete picture of population response, and may help to further refine cell type selectivity.

Receptor families with many receptors and ligands are often made up of a dense web of connections, making the role of individual components non-intuitive.[30,33] Interconnected, cross-reactive components may have evolved as a tradeoff between transmitting ligand-mediated information and expanding the repertoire of cell-surface proteins.[46] The methods outlined in this paper can be applied to many signaling systems characterized by pleiotropy and high-dimensionality. In addition to a detailed understanding of the important molecular regulatory connections, one must have a well-defined view of the desired cell response to achieve an optimal therapeutic effect. However, detailed biophysical and structural characterization, animal disease models, and evidence from human genetic studies make this engineering possible for therapies targeting other other complex signaling pathways such as Wnt, Hedgehog, Notch, and BMP/TGFβ.[30–33]

Methods

All analysis was implemented in Python, and can be found at https://github.com/meyer-lab/gc-cytokines, release 1.0.

Model

Base model

Cytokine (IL-2, -4, -7, -9, -15, & -21) binding to receptors was modeled using ordinary differential equations (ODEs). IL-2 and -15 each had two private receptors, one being a signaling-deficient α-chain (IL-2Rα & -15Rα) and the other being signaling-competent IL-2Rβ. The other four cytokines each had one signaling-competent private receptor (IL-7Rα, -9R, -4Rα, & -21Rα). JAK-STAT signaling is initiated when JAK-binding motifs are brought together. JAK binding sites are found on the intracellular regions of the γ_c, IL-2Rβ, IL-4Rα, IL-7Rα, IL-9R, and IL-21Rα receptors; therefore all complexes which contained two signaling-competent receptors were deemed to be active species. Ligands were assumed to first bind a private receptor and then can dimerize with other private receptors or γ_c thereafter. Direct binding of ligand to γ_c was not included due to its very weak or absent binding.[47]

In addition to binding interactions, our model incorporated receptor-ligand trafficking. Receptor synthesis was assumed to occur at a constant rate. The endocytosis rate was defined separately for active ($k_{endo,a}$) and inactive (k_{endo}) receptors. f_{sort} fraction of species in the endosome were ultimately trafficked to the lysosome, and active species in the endosome had a sorting fraction of 1.0. All endosomal species not sent to lysosomes were recycled back to the cell surface. The lysosomal degradation and recycling rate constants were defined as k_{deg} and k_{rec}, respectively. We assumed no autocrine ligand was produced by the cells. We assumed an endosomal volume of 10 fL and endosomal surface area half that of the plasma membrane.[43] All binding events were assumed to occur in the endosome with 5-fold greater disassociation rate due to its acidic pH.[29]

Free receptors and complexes were measured in units of number per cell and soluble ligands were measured in units of concentration (nM). Due to these unit choices for our species, the rate constants for ligand binding to a free receptors had units of nM^{-1} min^{-1}, rate constants for the forward dimerization of free receptor to complex had units of cell min^{-1} $number^{-1}$. Dissociation events had units of min^{-1}. All ligand-receptor binding processes had an assumed forward rate (k_{bnd}) of 10^7 M^{-1} sec^{-1}. All

forward dimerization reaction rates were assumed to be identical, represented by k_{fwd}. Reverse reaction rates were unique. Experimentally-derived affinities of 1.0,[26] 59,[48] 0.1,[49] and 0.07 nM[26] were used for IL-4, -7, -9, and -21 binding to their cognate private receptors, respectively. IL-2 and -15 were assumed to have affinities of 10 nM and 0.065 nM for their respective α-chains,[50–52] and an affinity of 144 and 438 nM for their respective β-chains.[50] Rates k_5, k_{10}, and k_{11} were set to their experimentally-determined dissassociation constants of 1.5, 12, and 63 nM.[50]

Initial values were calculated by assuming steady-state in the absence of ligand. Differential equation solving was performed using the SUNDIALS solvers in C++, with a Python interface for all other code.[53] Model sensitivities were calculated using the adjoint solution.[54] Calculating the adjoint requires the partial derivatives of the differential equations both with respect to the species and unknown parameters. Constructing these can be tedious and error-prone. Therefore, we calculated these algorithmically using forward-pass autodifferentiation implemented in Adept-2.[55] A model and sensitivities tolerance of 10^{-9} and 10^{-3}, respectively, were used throughout. We used unit tests for conservation of mass, equilibrium, and detailed balance to help ensure model correctness.

Model fitting

We used Markov chain Monte Carlo to fit the unknown parameters in our model using previously published cytokine response data.[14,26] Experimental measurements include pSTAT activity under stimulation with varying concentrations of IL-2, -15, -4, and -7 as well as time-course measurements of surface IL-2Rβ upon IL-2 and -15 stimulation. YT-1 human NK cells were used for all data-sets involving IL-2 and IL-15. Human PBMC-derived CD4+TCR+CCR7^{high} cells were used for all IL-4 and -7 response data. All YT-1 cell experiments were performed both with the wild-type cell line, lacking IL-2Rα, and cells sorted for appreciable expression of the receptor. Data from Ring *et al* and Gonnord *et al* can be found in Figure 5 and Figure S3, respectively.[14,26] Measurements of receptor counts at steady state in Gonnord *et al* were used to solve for IL-7Rα, IL-4Rα, and γ_c expression rates in human PBMCs.

Fitting was performed with the Python package PyMC3. All unknown rate parameters were assumed to have a lognormal distribution with a standard deviation of 0.1; the only exception to these distributions was f_{sort} which was assumed to have a beta distribution with shape parameters of α=20 and β=40. Executing this fitting process yielded likelihood distributions of each unknown parameter and sum of squared error between model prediction and experimental data at each point of experimental data. The Geweke criterion metric was used to verify fitting convergance for all versions of the model (Fig. S2).[56]

Tensor Generation and Factorization

To perform factorization of model predictions, we generated a three-dimensional (timepoints $\times$ cell types $\times$ ligand) data tensor of predicted ligand-induced signaling. We predicted simulating 10 cell types with IL-2, IL-7, IL-15, or a mutant IL-2Rα affinity-enriched IL-2. The receptor expression rates were set based on measured surface abundance (Fig. 3B). The ligand stimulation concentrations matched those from our experiments (Fig. S5D). Before decomposition, the tensor was variance scaled across each cell population. Tensor decomposition was performed using the Python package TensorLy.[57] The number of components was set based on the minimum required number to reconstruct >95% of the variance in the original tensor (R2X).

Experimental Methods

Receptor abundance quantitation

Cryopreserved PBMCs (ATCC, PCS-800-011, lot#81115172) were thawed to room temperature and slowly diluted with 9 mL pre-warmed RPMI-1640 medium (Gibco, 11875-093) supplemented with 10% fetal bovine serum (FBS, Seradigm, 1500-500, lot#322B15). Media was removed, and cells washed once more with 10 mL warm RPMI-1640 + 10% FBS. Cells were brought to 1.5×10^6 cells/mL, distributed at 250,000 cells per well in a 96-well V-bottom plate, and allowed to recover 2 hrs at 37°C in an incubator at 5% CO2. Cells were then washed twice with PBS + 0.1% BSA (PBSA,

414 Gibco, 15260-037, Lot#2000843) then suspended in 50 µL PBSA + 10% FBS for 10
415 min on ice to reduce background binding to IgG.

416 Antibodies were diluted in PBSA + 10% FBS and cells were stained for 1 hr at 4°C
417 in darkness with a gating panel (Panel 1, Panel 2, Panel 3, or Panel 4) and one anti-
418 receptor antibody, or an equal concentration of matched isotype/fluorochrome control
419 antibody. Stain for CD25 was included in Panel 1 when CD122, CD132, CD127, or
420 CD215 was being measured (CD25 is used to separate T_{reg}s from other CD4+ T cells).

421 Compensation beads (Simply Cellular Compensation Standard, Bangs Labs, 550,
422 lot#12970) and quantitation standards (Quantum Simply Cellular anti-Mouse IgG
423 or anti-Rat IgG, Bangs Labs, 815, Lot#13895, 817, Lot#13294) were prepared for
424 compensation and standard curve. One well was prepared for each fluorophore with
425 2 µL antibody in 50 µL PBSA and the corresponding beads. Bead standards were
426 incubated for 1 hr at room temperature in the dark.

427 Both beads and cells were washed twice with PBSA. Cells were suspended in 120 µL
428 per well PBSA, and beads to 50 µL, and analyzed using an IntelliCyt iQue Screener
429 PLUS with VBR configuration (Sartorius) with a sip time of 35 and 30 secs for cells and
430 beads, respectively. Antibody number was calculated from fluorescence intensity by
431 subtracting isotype control values from matched receptor stains and calibrated using
432 the two lowest binding quantitation standards. T_{reg} cells could not be gated in the
433 absence of CD25, so CD4+ T cells were used as the isotype control to measure CD25 in
434 T_{reg} populations. Cells were gated as shown in Fig. S3. Measurements were performed
435 using four independent staining procedures over two days. Separately, the analysis
436 was performed with anti-receptor antibodies at 3x normal concentration to verify that
437 receptor binding was saturated. Replicates were summarized by geometric mean.

438 **pSTAT5 Measurement of IL-2 and -15 Signaling in PBMCs**

439 Human PBMCs were thawed, distributed across a 96-well plate, and allowed to recover
440 as described above. IL-2 (R&D Systems, 202-IL-010) or IL-15 (R&D Systems, 247-ILB-
441 025) were diluted in RPMI-1640 without FBS and added to the indicated concentrations.
442 To measure pSTAT5, media was removed, and cells fixed in 100 µL of 10% formalin

(Fisher Scientific, SF100-4) for 15 mins at room temperature. Formalin was removed, cells were placed on ice, and cells were gently suspended in 50 µL of cold methanol (-30℃). Cells were stored overnight at -30℃. Cells were then washed twice with PBSA, split into two identical plates, and stained 1 hr at room temperature in darkness using antibody panels 4 and 5 with 50 µL per well. Cells were suspended in 100 µL PBSA per well, and beads to 50 µL, and analyzed on an IntelliCyt iQue Screener PLUS with VBR configuration (Sartorius) using a sip time of 35 seconds and beads 30 seconds. Compensation was performed as above. Populations were gated as shown in Fig. S3, and the median pSTAT5 level extracted for each population in each well.

Acknowledgements

This work was supported by NIH DP5-OD019815 to A.S.M. **Competing financial interests:** S.M.C. and C.P. are employees of Visterra Inc.

Author contributions statement

A.S.M. and S.M.C. conceived of the study. S.M.C. and C.P. performed the PBMC experiments. A.C.W., A.M.F., A.S.M, and Z.S.K. performed the computational analysis. All authors helped to design experiments and/or analyze the data.

Supplement

IL-2, IL-15, and IL-7 Receptor Quantitation

Table S1: Antibodies used to quantify receptors and cell types.

Antibody (clone)	Dilution	Fluorophore	Vendor (CAT#)	Panel[†]
CD25 (M-A251)	1:120	Brilliant Violet 421	BioLegend (356114)	0
CD122 (TU27)	1:120	PE/Cy7	BioLegend (339014)	0
CD132 (TUGh4)	1:120	APC	BioLegend (3386	0
CD215 1st mAb (JM7A4)	1:120	APC	BioLegend (330210)	0
CD215 2nd mAb (151303)	3:100	APC	R&D Systems (FAB1471A)	0
CD127 (A019D5)	1:120	Alexa Fluor 488	BioLegend (351313)	0
Ms IgG1κ (MOPC-21)	1:240	Brilliant Violet 421	BioLegend (400158)	0
Md IgG1κ (MOPC-21)	1:240	PE/Cy7	BioLegend (400126)	0
Rat IgG2Bκ (RTK4530)	1:60	APC	BioLegend (400612)	0
Ms IgG2Bκ (MPC-11)	1:120	APC	BioLegend (400320)	0
Ms IgG2B (133303)	3:100	APC	R&D Systems (IC0041A)	0
Ms IgG1κ (MOPC-21)	1:120	Alexa Fluor 488	BioLegend (400129)	0
CD3 (UCHT1)	1:120	Brilliant Violet 605	BioLegend (300460)	1
CD4 (RPA-T4)	1:120	Brilliant Violet 785	BioLegend (300554)	1
CD127 (A019D5)	1:120	Alexa Fluor 488	BioLegend (351313)	1
CD45RA (HI100)	1:120	PE/Dazzle 594	BioLegend (304146)	1
CD3 (UCHT1)	1:120	Brilliant Violet 605	BioLegend (300460)	2
CD56 (5.1H11)	1:120	PE/Dazzle 594	BioLegend (362544)	2
CD3 (UCHT1)	1:120	Brilliant Violet 605	BioLegend (300460)	3
CD8 (RPA-T8)	1:120	Brilliant Violet 785	BioLegend (301046)	3
CD45RA (HI100)	1:120	PE/Dazzle 594	BioLegend (304146)	3
CD25 (M-A251)	1:120	Brilliant Violet 421	BioLegend (356114)	4
CD3 (UCHT1)	1:120	Brilliant Violet 605	BioLegend (300460)	4
CD4 (RPA-T4)	1:120	Brilliant Violet 785	BioLegend (300554)	4
CD127 (A019D5)	1:120	Alexa Fluor 488	BioLegend (351313)	4

Antibody (clone)	Dilution	Fluorophore	Vendor (CAT#)	Panel[†]
CD45RA (HI100)	1:120	PE/Dazzle 594	BioLegend (304146)	4
CD56 (5.1H11)	1:120	PE/Cy7	BioLegend (362510)	4
CD8 (RPA-T8)	1:120	Alexa Fluor 647	BioLegend (301062)	4
Foxp3 (259D)	1:50	Alexa Fluor 488	BioLegend (320212)	5
CD25 (M-A251)	1:120	Brilliant Violet 421	BioLegend (356114)	5
CD4 (SK3)	1:120	Brilliant Violet 605	BioLegend (344646)	5
CD45RA (HI100)	1:120	PE/Dazzle 594	BioLegend (304146)	5
pSTAT5 (C71E5)	1:120	Alexa Fluor 647	CST[*] (9365)	5
CD3 (UCHT1)	1:120	Brilliant Violet 605	BioLegend (300460)	6
CD8 (RPA-T8)	1:120	Alexa Fluor 647	BioLegend (301062)	6
CD56 (5.1H11)	1:120	Alexa Fluor 488	BioLegend (362518)	6
pSTAT5 (D4737)	1:120	PE	CST[*] (14603)	6

[*]CST: Cell Signaling Technology

[†]*Panel 0:* Antibodies for IL-2, IL-15, and IL-7 receptor analysis; *Panel 1:* Antibodies to gate Naïve and Memory T-regulatory and T-helper cells; *Panel 2:* Antibodies to gate NK and CD56bright NK cells; *Panel 3:* Antibodies to gate Naïve and Memory Cytotoxic T cells; *Panel 4:* Antibodies to gate Naïve and Memory T-regulatory, T helper, and Cytotoxic cells, and NK cells for CD127 (IL-7) Quantitation; *Panel 5:* Antibodies to gate Memory and Naïve T-regulatory cells, Memory and Naïve T-helper cells; *Panel 6:* Antibodies to gate NK cells, CD56bright NK cells, and Cytotoxic T cells

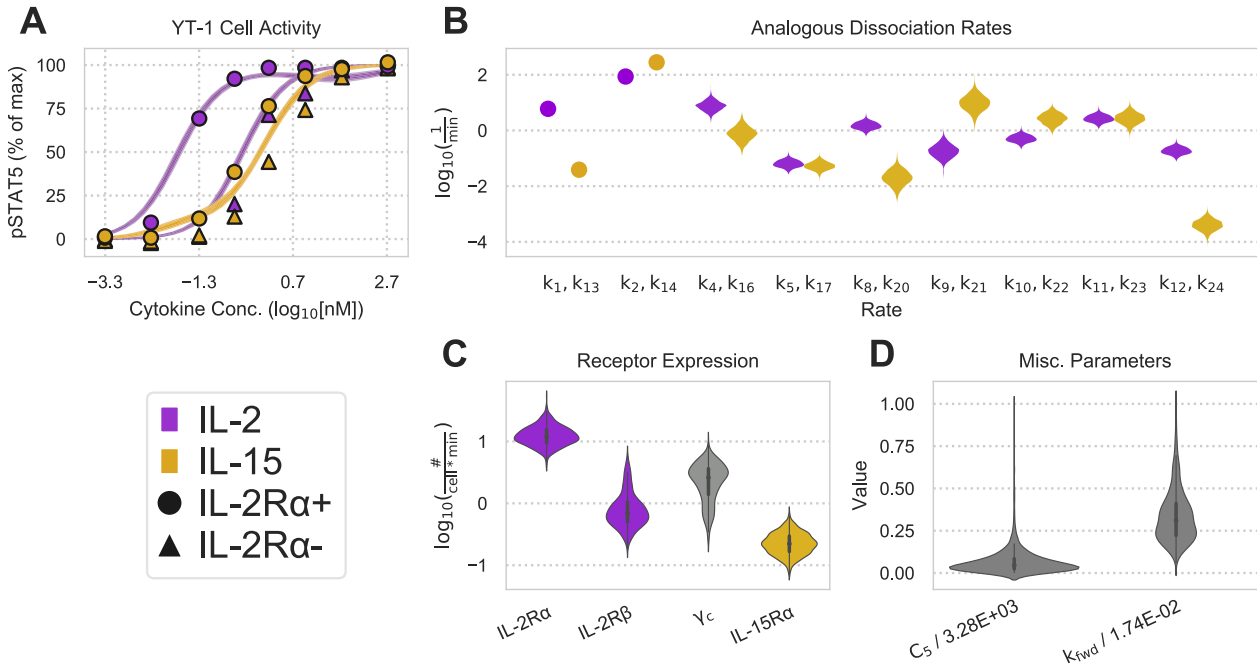

Figure S1: **Model without trafficking fails to capture IL-2/-15 dose response.** A) Model without trafficking fit to IL-2 and IL-15 pSTAT5 dose response data.[14] This model was not fit to the surface IL-2Rβ measurements since no receptors were allowed to internalize from the cell surface (Fig. 1B-D). B) Posterior distributions of analogous reverse reaction rates for IL-2 and IL-15 in no-trafficking model. C) Posterior distributions for receptor surface abundance in no-trafficking model. D) Posterior distribution for the pSTAT5 activity scaling constant in no-trafficking model.

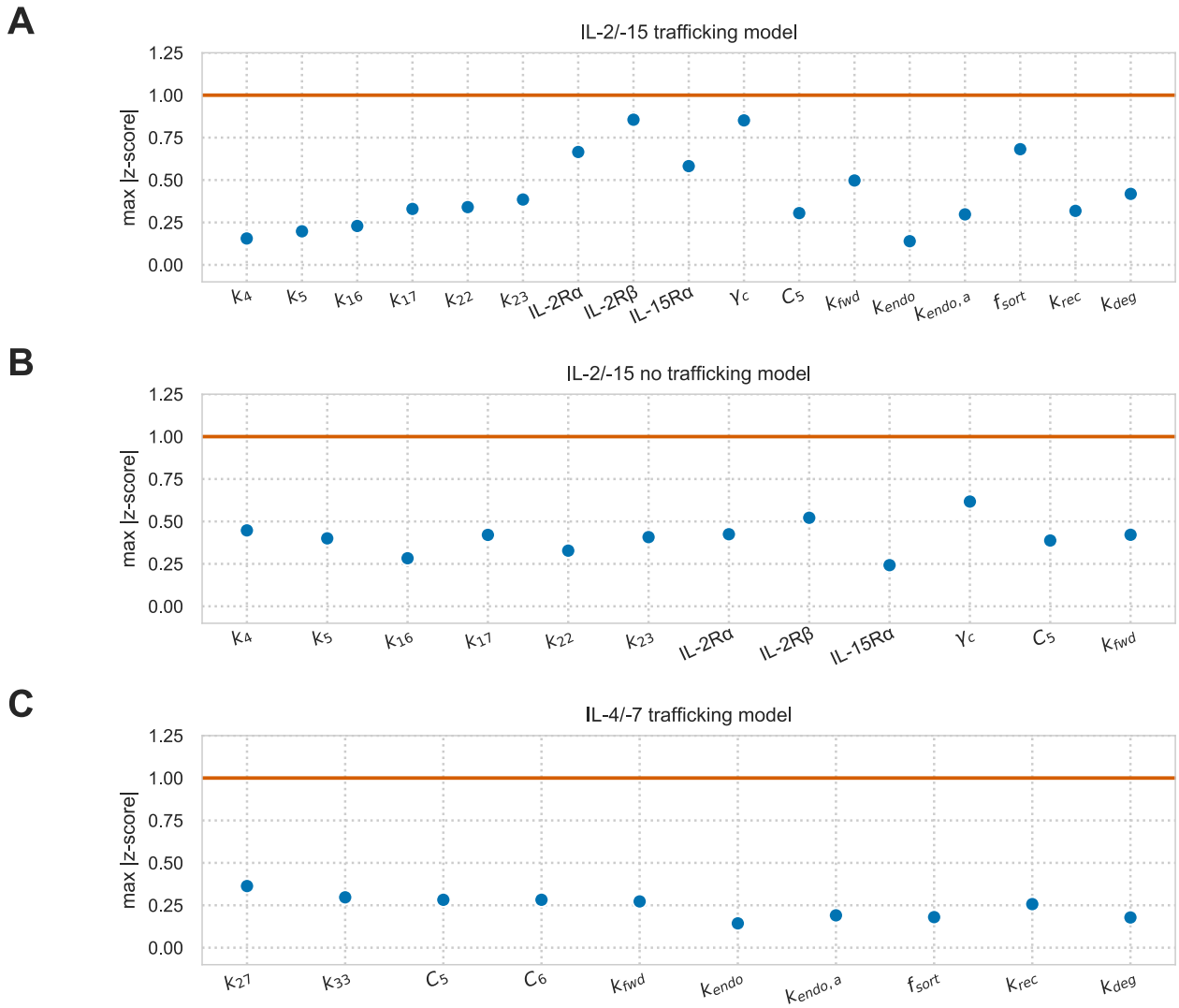

Figure S2: **Geweke criterion scores for model fitting with and without trafficking.** Geweke criterion z-scores in all subplots were calculated using 20 intervals in the first 10% and last 50% of MCMC chain. The interval with the highest absolute z-score was plotted for each parameter. Scores of $|z| < 1$ imply fitting convergence. A-B) IL-2/-15 with and without trafficking. C) IL-4/-7 with trafficking (Fig. S1).

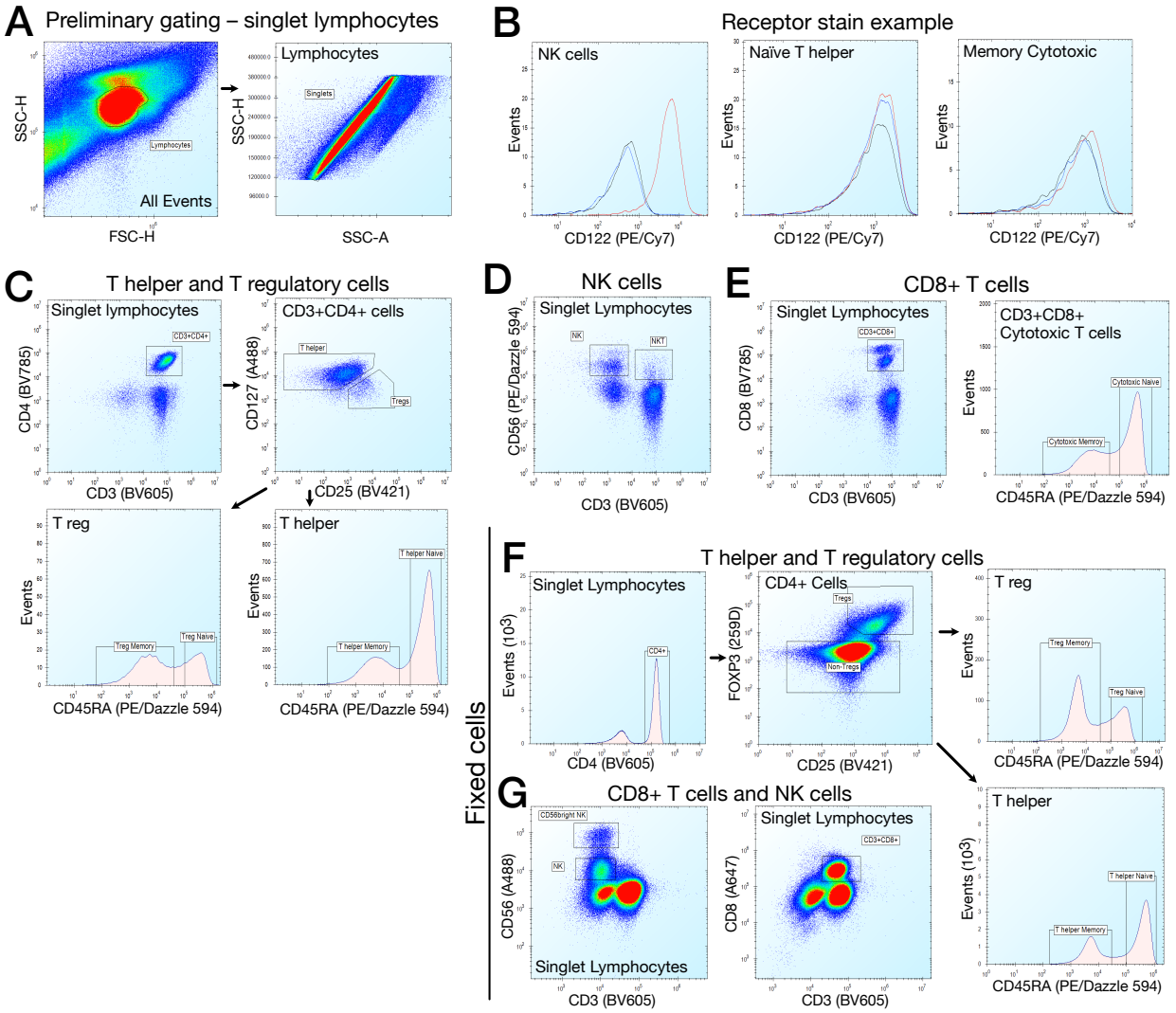

Figure S3: **Receptor quantification and gating of PBMC-derived immune cell types.** A) Preliminary gating for singlet lyphocytes. B) Example staining for CD122 (red), the corresponding isotype control (blue), and unstained cells (black). C) Gating for live T helper and T regulatory cells during receptor quantification. D) Live cell NK cell gating. E) Live cell CD8+ T cell gating. F) Gating for fixed T helper and T regulatory cells during pSTAT5 quantification. G) Fixed CD8+ T cell and NK cell gating.

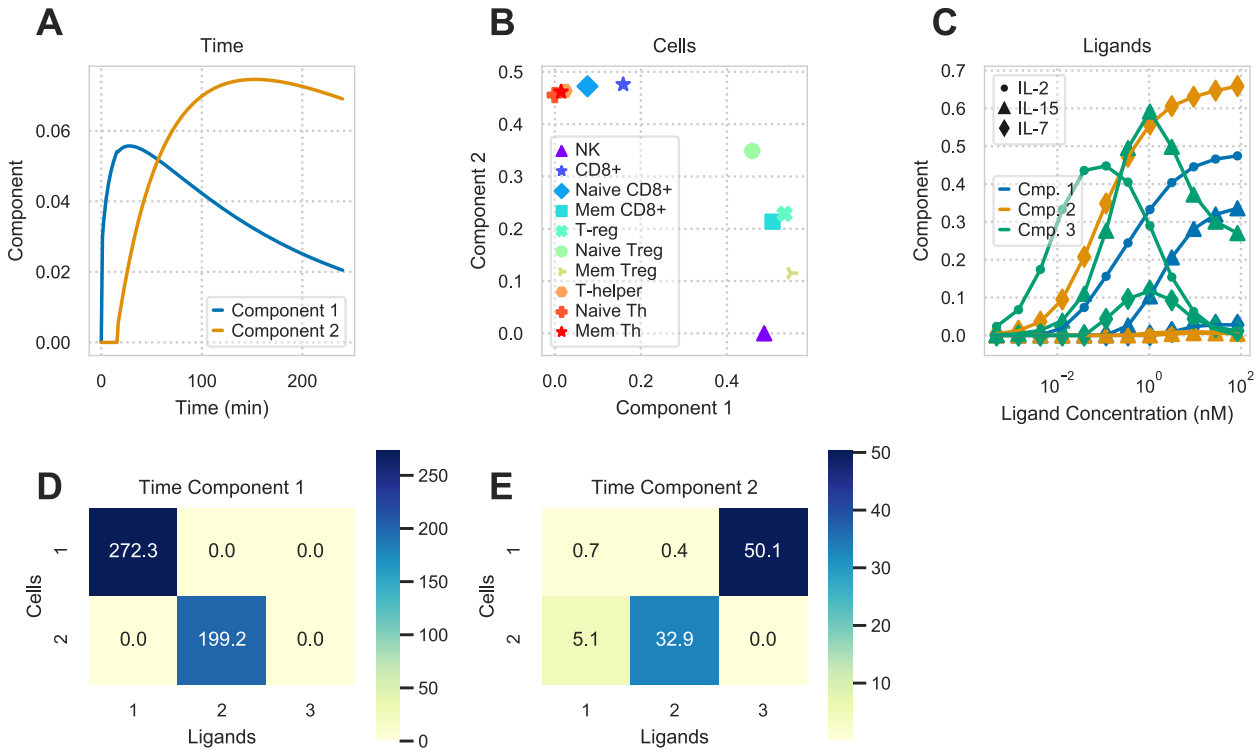

Figure S4: **Tucker factorization of predicted immune cell type responses.** A) Timepoint decomposition plot showing factorization component values against time after decomposing the tensor's first dimension into 2 components. B) Decomposition plot along the second (cell) dimension after decomposing it to 2 components showing the ten cell type values along each component. C) Ligand decomposition plot along the tensor's third dimension after decomposing it into 3 components. D–E) Slices of the Tucker core tensor corresponding to time component 1 (D) and 2 (E).

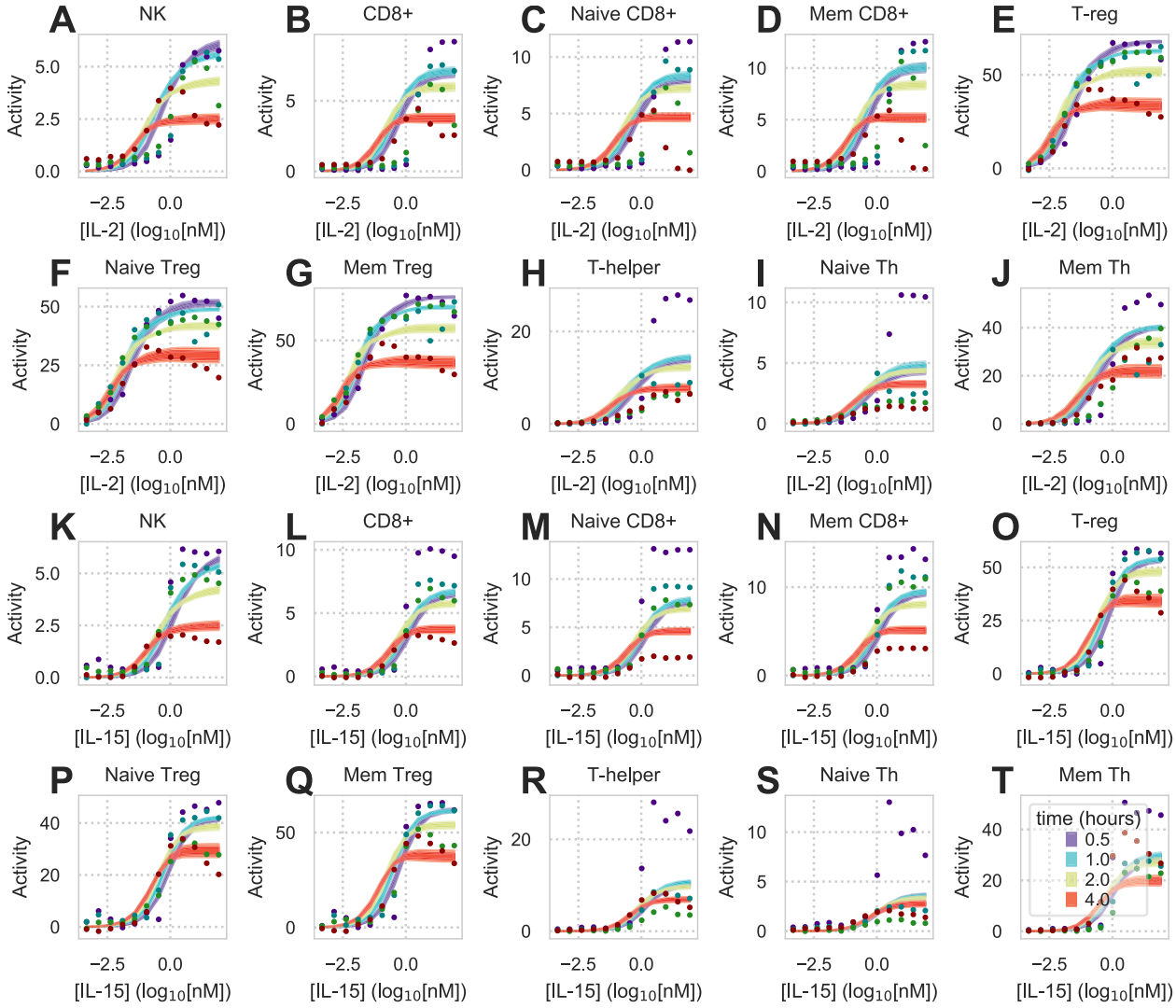

Figure S5: **Full panel of predicted versus actual immune cell type responses.** Dots represent experimental measurements and shaded regions represent 10-90% confidence interval for model predictions. Time of pSTAT5 activity measurement is denoted by color. All cell populations were stimulated with either IL-2 (A-J) or IL-15 (K-T).

References

1. Rochman, Y., Spolski, R. & Leonard, W. New insights into the regulation of T cells by γc family cytokines. *Nature Reviews Immunology* **9**, 480–490 (2009).

2. Leonard, W. J., Lin, J.-X. & O'Shea, J. J. The γc family of cytokines: Basic biology to therapeutic ramifications. *Immunity* **50**, 832–850 (2019).

3. Walsh, S. T. R. A biosensor study indicating that entropy, electrostatics, and receptor glycosylation drive the binding interaction between interleukin-7 and its receptor. *Biochemistry* **49**, 8766–8778 (2010).

4. Amorosi, S. *et al.* The cellular amount of the common γ-chain influences spontaneous or induced cell proliferation. *The Journal of Immunology* **182**, 3304–3309 (2009).

5. Vigliano, I. *et al.* Role of the common γ chain in cell cycle progression of human malignant cell lines. *International Immunology* **24**, 159–167 (2012).

6. Wang, L. *et al.* Key role for IL-21 in experimental autoimmune uveitis. *Proceedings of the National Academy of Sciences* **108**, 9542–9547 (2011).

7. Sharma, R. *et al.* Cutting edge: A regulatory t cell-dependent novel function of cd25 (il-2Rα) controlling memory cd8+ t cell homeostasis. *The Journal of Immunology* **178**, 1251–1255 (2007).

8. Sharfe, N., Dadi, H. K., Shahar, M. & Roifman, C. M. Human immune disorder arising from mutation of the α chain of the interleukin-2 receptor. *Proceedings of the National Academy of Sciences* **94**, 3168–3171 (1997).

9. Horak, I. Immunodeficiency in il-2-knockout mice. *Clin Immunol Immunopathol* **76**, S172–3

10. Human il2ra null mutation mediates immunodeficiency with lymphoproliferation and autoimmunity. *Clinical Immunology* **146**, 248–261 (2013).

11. Stephanie R. Pulliam, S. E. A., Roman V. Uzhachenko & Shanker, A. Common gamma chain cytokines in combinatorial immune strategies against cancer. *Immunology letters* **169**, 61–72 (2015).

12. Bentebibel, S.-E. *et al.* A first-in-human study and biomarker analysis of NKTR-214, a novel IL-2-receptor beta/gamma (βγ)-biased cytokine, in patients with advanced or metastatic solid tumors. *Cancer Discovery* (2019). doi:10.1158/2159-8290.CD-18-1495

13. Zhu, E. F. *et al.* Synergistic innate and adaptive immune response to combination immunotherapy with anti-tumor antigen antibodies and extended serum half-life il-2. *Cancer Cell* **27**, 489–501

14. Ring, A. M. *et al.* Mechanistic and structural insight into the functional dichotomy between IL-2 and IL-15. *Nature Immunology* **13**, 1187–1195 (2012).

15. Cotari, J. W., Voisinne, G., Dar, O. E., Karabacak, V. & Altan-Bonnet, G. Cell-to-cell variability analysis dissects the plasticity of signaling of common γ chain cytokines in T cells. *Science Signaling* **6**, ra17–ra17 (2013).

16. Krieg, C., Letourneau, S., Pantaleo, G. & Boyman, O. Improved IL-2 immunotherapy by selective stimulation of IL-2 receptors on lymphocytes and endothelial cells. *Proc Natl Acad Sci U S A* **107**, 11906–11911

17. Konrad, M. W. *et al.* Pharmacokinetics of recombinant interleukin 2 in humans. *Cancer Research* **50**, 2009–2017 (1990).

18. Bernett, M. J. *et al.* Abstract 1595: IL-15/IL-15Rα heterodimeric Fc-fusions with extended half-lives. *Cancer Research* **77**, 1595–1595 (2017).

19. William G. Berndt, K. A. S., David Z. Chang & Ciardelli, T. L. Mutagenic analysis of a receptor contact site on interleukin-2: Preparation of an IL-2 analog with increased potency. *Biochemistry* **33**, 6571–6577

20. Collins, L. *et al.* Identification of specific residues of human interleukin 2 that affect binding to the 70-kDa subunit (p70) of the interleukin 2 receptor. *Proceedings of the National Academy of Sciences* **85**, 7709–7713 (1988).

21. Aron M. Levin, A. M. R., Darren L. Bates. Exploiting a natural conformational switch to engineer an interleukin-2 'superkine'. *Nature* **484**, 529–533 (2012).

22. Bell, C. J. M. *et al.* Sustained *in vivo* signaling by long-lived IL-2 induces prolonged increases of regulatory T cells. *Journal of Autoimmunity* **56**, 66–80 (2015).

23. Peterson, L. B. *et al.* A long-lived IL-2 mutein that selectively activates and expands regulatory T cells as a therapy for autoimmune disease. *Journal of Autoimmunity* **95**, 1–14 (2018).

24. Burke, M. A. *et al.* Modeling the proliferative response of T cells to IL-2 and IL-4. *Cellular Immunology* **178**, 42–52 (1997).

25. Feinerman, O. *et al.* Single-cell quantification of IL-2 response by effector and regulatory T cells reveals critical plasticity in immune response. *Molecular Systems Biology* **6**, (2010).

26. Gonnord, P. *et al.* A hierarchy of affinities between cytokine receptors and the common gamma chain leads to pathway cross-talk. *Science Signaling* **11**, (2018).

27. Duprez, V., Cornet, V. & Dautry-Varsat, A. Down-regulation of high affinity interleukin 2 receptors in a human tumor T cell line. Interleukin 2 increases the rate of surface receptor decay. *Journal of Biological Chemistry* **263**, 12860–12865 (1988).

28. Lamaze, C. *et al.* Interleukin 2 receptors and detergent-resistant membrane domains define a clathrin-independent endocytic pathway. *Molecular Cell* **7**, 661–671 (2001).

29. Fallon, E. M. & Lauffenburger, D. A. Computational model for effects of ligand/receptor binding properties on interleukin-2 trafficking dynamics and T cell proliferation response. *Biotechnology Progress* **16**, 905–916

30. Eubelen, M. *et al.* A molecular mechanism for Wnt ligand-specific signaling. *Science* **361**, (2018).

31. Li, P. *et al.* Morphogen gradient reconstitution reveals Hedgehog pathway design principles. *Science* **360**, 543–548 (2018).

32. Antebi, Y. E., Nandagopal, N. & Elowitz, M. B. An operational view of intercellular signaling pathways. *Current Opinion in Systems Biology* **1**, 16–24 (2017).

33. Antebi, Y. E. *et al.* Combinatorial signal perception in the BMP pathway. *Cell* **170**, 1184–1196

34. Fallon, E. M., Liparoto, S. F., Lee, K. J., Ciardelli, T. L. & Lauffenburger, D. A. Increased

endosomal sorting of ligand to recycling enhances potency of an interleukin-2 analog. *Journal of Biological Chemistry* **275**, 6790–6797 (2000).

35. Basquin, C. *et al.* The signalling factor PI3K is a specific regulator of the clathrin-independent dynamin-dependent endocytosis of IL-2 receptors. *Journal of Cell Science* **126**, 1099–1108 (2013).

36. Mitra, S. *et al.* Interleukin-2 activity can be fine tuned with engineered receptor signaling clamps. *Immunity* **42**, 826–838 (2015).

37. Spangler, J. B. *et al.* Antibodies to interleukin-2 elicit selective T cell subset potentiation through distinct conformational mechanisms. *Immunity* **42**, 815–825 (2015).

38. Hassan, J. & Reen, D. J. IL-7 promotes the survival and maturation but not differentiation of human post-thymic CD4+ T cells. *European journal of immunology* **28**, 3057–3065 (1998).

39. Tucker, L. R. Some mathematical notes on three-mode factor analysis. *Psychometrika* **31**, 279–311 (1966).

40. Junghans, R. P. & Waldmann, T. A. Metabolism of tac (IL2Ralpha): Physiology of cell surface shedding and renal catabolism, and suppression of catabolism by antibody binding. *Journal of Experimental Medicine* **183**, 1587–1602 (1996).

41. Kuwabara, T., Kasai, H. & Kondo, M. Acetylation modulates IL-2 receptor signaling in T cells. *Journal of Immunology* **197**, 4334–4343 (2016).

42. Haugh, J. M. Mathematical model of human growth hormone (hGH)-stimulated cell proliferation explains the efficacy of hGH variants as receptor agonists or antagonists. *Biotechnology Progress* **20**, 1337–1344

43. Meyer, A. S., Zweemer, A. J. & Lauffenburger, D. A. The AXL receptor is a sensor of ligand spatial heterogeneity. *Cell Systems* **1**, 25–36 (2015).

44. León, K., García-Martínez, K., Carmenate, T. & Rojas, G. Combining computational and experimental biology to develop therapeutically valuable IL2 muteins. *Seminars in Oncology* **45**, 95–104 (2018).

45. Leon, K., Garcia-Martinez, K. & Carmenate, T. Mathematical models of the impact of

IL-2 modulation therapies on T cell dynamics. *Frontiers in Immunology* **4**, 439 (2013).

46. Komorowski, M. & Tawfik, D. S. The limited information capacity of cross-reactive sensors drives the evolutionary expansion of signaling. *Cell Systems* **8**, 76–85.e6 (2019).

47. Voss, S. D., Leary, T. P., Sondel, P. M. & Robb, R. J. Identification of a direct interaction between interleukin 2 and the p64 interleukin 2 receptor gamma chain. *Proceedings of the National Academy of Sciences* **90**, 2428–2432 (1993).

48. Walsh, S. T. R. Structural insights into the common γ-chain family of cytokines and receptors from the interleukin-7 pathway. *Immunological Reviews* **250**, 303–316

49. Renauld, J. C. *et al.* Expression cloning of the murine and human interleukin 9 receptor cDNAs. *Proceedings of the National Academy of Sciences* **89**, 5690–5694 (1992).

50. Rickert, M., J Boulanger, M., Goriatcheva, N. & Christopher Garcia, K. Compensatory energetic mechanisms mediating the assembly of signaling complexes between interleukin-2 and its α, β, and γc receptors. *Journal of molecular biology* **339**, 1115–28 (2004).

51. Mortier, E. *et al.* Soluble interleukin-15 receptor α (IL-15Rα)-sushi as a selective and potent agonist of IL-15 action through IL-15Rβ/γ: Hyperagonist IL-15·IL-15Rα fusion proteins. *Journal of Biological Chemistry* **281**, 1612–1619 (2006).

52. Dubois, S., Mariner, J., Waldmann, T. A. & Tagaya, Y. IL-15Rα recycles and presents IL-15 in *trans* to neighboring cells. *Immunity* **17**, 537–547 (2002).

53. Hindmarsh, A. C. *et al.* SUNDIALS: Suite of nonlinear and differential/algebraic equation solvers. *ACM Transactions on Mathematical Software (TOMS)* **31**, 363–396 (2005).

54. Cao, Y., Li, S. & Petzold, L. Adjoint sensitivity analysis for differential-algebraic equations: Algorithms and software. *Journal of Computational and Applied Mathematics* **149**, 171–191 (2002).

55. Hogan, R. J. Adept 2.0: a combined automatic differentiation and array library for C++. (2017). doi:10.5281/zenodo.1004730

56. Geweke, J. Evaluating the accuracy of sampling-based approaches to the calculation of posterior moments. in *Bayesian statistics 4* 169–193 (University Press, 1992).

57. Kossaifi, J., Panagakis, Y. & Pantic, M. TensorLy: Tensor learning in Python. *CoRR* **abs/1610.09555**, (2016).